Transcriptome and proteome analyses reveal that upregulation of GSTM2 by allisartan improves cardiac remodeling and dysfunction in hypertensive rats

HAO WU[1,2], YAJUN ZHAI[3], JING YU[4], LIPING WEI[1,2] and XIN QI[1,2]

[1]School of Medicine, Nankai University, Tianjin 300071; [2]Department of Cardiology, Tianjin Union Medical Center, Tianjin 300121; [3]Graduate School; [4]Department of Physiology and Pathophysiology, Tianjin Medical University, Tianjin 300070, P.R. China

Received October 3, 2023; Accepted February 20, 2024

DOI: 10.3892/etm.2024.12508

Abstract. Long-term hypertension can lead to hypertensive heart disease, which ultimately progresses to heart failure. As an angiotensin receptor blocker antihypertensive drug, allisartan can control blood pressure, and improve cardiac remodeling and cardiac dysfunction caused by hypertension. The aim of the present study was to investigate the protective effects of allisartan on the heart of spontaneously hypertensive rats (SHRs) and the underlying mechanisms. SHRs were used as an animal model of hypertensive heart disease and were treated with allisartan orally at a dose of 25 mg/kg/day. The blood pressure levels of the rats were continuously monitored, their body and heart weights were measured, and their cardiac structure and function were evaluated using echocardiography. Wheat germ agglutinin staining and Masson trichrome staining were employed to assess the morphology of the myocardial tissue. In addition, transcriptome and proteome analyses were performed using the Solexa/Illumina sequencing platform and tandem mass tag technology, respectively. Immunofluorescence co-localization was conducted to analyze Nrf2 nuclear translocation, and TUNEL was performed to detect the levels of cell apoptosis. The protein expression levels of pro-collagen I, collagen III, phosphorylated (p)-AKT, AKT, p-PI3K and PI3K, and the mRNA expression levels of Col1a1 and Col3a1 were determined by western blotting and reverse transcription-quantitative PCR, respectively. Allisartan lowered blood pressure, attenuated cardiac remodeling and improved cardiac function in SHRs. In addition, allisartan alleviated cardiomyocyte hypertrophy and cardiac fibrosis. Allisartan also significantly affected the 'pentose phosphate pathway', 'fatty acid elongation', 'valine, leucine and isoleucine degradation', 'glutathione metabolism', and 'amino sugar and nucleotide sugar metabolism' pathways in the hearts of SHRs, and upregulated the expression levels of GSTM2. Furthermore, allisartan activated the PI3K-AKT-Nrf2 signaling pathway and inhibited cardiomyocyte apoptosis. In conclusion, the present study demonstrated that allisartan can effectively control blood pressure in SHRs, and improves cardiac remodeling and cardiac dysfunction. Allisartan may also upregulate the expression levels of GSTM2 in the hearts of SHRs and significantly affect glutathione metabolism, as determined by transcriptome and proteome analyses. The cardioprotective effect of allisartan may be mediated through activation of the PI3K-AKT-Nrf2 signaling pathway, upregulation of GSTM2 expression and reduction of cardiomyocyte apoptosis in SHRs.

Correspondence to: Professor Xin Qi, Department of Cardiology, Tianjin Union Medical Center, 190 Jieyuan Road, Tianjin 300121, P.R. China
E-mail: qixinx2011@yeah.net

Key words: allisartan, GSTM2, Nrf2, cardiac remodeling, hypertension

Introduction

Hypertension is a major modifiable risk factor for cardiovascular disease (CVD) and premature mortality worldwide (1). It has been shown that long-term hypertension can cause hypertensive heart disease, which is characterized by increased left ventricular pressure load, resulting in pathological changes in cardiac structure and function, such as left ventricular hypertrophy, myocardial fibrosis and left ventricular remodeling, which can eventually lead to heart failure (2). Cardiac fibrosis is a common pathological change at the late stage of CVD, which is characterized by an imbalance in the ratio of cardiomyocytes, cardiac fibroblasts and collagen, as well as excessive production and deposition of the extracellular matrix (ECM), resulting in the formation of scar tissue and leading to pathological changes in cardiac structure and dysfunction in myocardial contraction and relaxation (3).

Allisartan is a new antihypertensive drug that works by blocking the angiotensin (Ang) II receptor, which was discovered and developed in China (4). Compared with losartan, allisartan ester can be completely hydrolyzed by esterases into its active metabolite EXP3174 after absorption by the small intestine and stomach (5,6). The active metabolite can then specifically bind to Ang II receptor type 1, blocking the

physiological effects of Ang II, thereby lowering blood pressure and protecting target organs from damage. The beneficial effects of Ang receptor blocker (ARBs) in improving cardiac remodeling and heart failure by inhibiting the renin-Ang-aldosterone system (RAAS) are well known (7). However, as an ARB drug, allisartan may have additional mechanisms beyond blood pressure control. Allisartan has been shown to inhibit NAD(P)H oxidase expression, providing protection for the cerebrovascular system, heart and aorta (4). There is also evidence that the antioxidative and anti-inflammatory effects of allisartan may be related to the SIRT1/Nrf2/NF-κB signaling pathway (6). Allisartan can also regulate the expression of voltage-gated potassium channels, Kv7 (8) and Kv1.5 (9), in hypertensive rats. Therefore, in-depth exploration of the mechanisms of action of allisartan may improve understanding of the pathogenesis of hypertensive heart disease and result in the identification of new therapeutic targets.

GSTM2 belongs to the GST family and functions in detoxifying reactive oxygen species (ROS) (10). A dysregulation between the production of ROS and the endogenous antioxidant defense mechanisms is known as oxidative stress (11). Oxidative stress serves a role in the development and progression of cardiac remodeling and cardiac dysfunction (12). GSTM2 protects cells from oxidative stress-related damage and cell death by participating in the clearance of ROS (10). Additional research has shown that GSTM2 regulates autophagy (13,14) and exerts protective effects against arrhythmia (15) and cellular aging (16) through alternative mechanisms.

The present study analyzed differentially expressed genes and proteins in the heart tissue of WKY, spontaneously hypertensive rat (SHR) and SHR + allisartan groups using transcriptome and proteome analyses. It was hypothesized that allisartan could affect the expression of GSTM2 and improve the development of hypertension through the PI3K-AKT-Nrf2 signaling pathway. The present study may provide a new therapeutic strategy for the clinical treatment of hypertension and expand the clinical application of allisartan.

Material and methods

Animals and groups. SHRs are the most commonly used rat model of human essential hypertension (17-19), which spontaneously develops elevated blood pressure when fed a normal diet. The SHR strain originated in Kyoto, Japan, through the breeding of an outbred Wistar male rat, displaying spontaneously elevated blood pressure, with a female rat exhibiting slightly elevated blood pressure. Subsequent brother-sister mating was sustained, focusing on selecting animals with systolic blood pressure >150 mmHg (20). The inbred strain was established in the United States in the late 1960s after undergoing 20 generations of inbreeding at the National Institutes of Health. These rats spontaneously develop hypertension during adulthood (21). Normotensive WKY rats (n=10; age, 13 weeks; Beijing Vital River Laboratory Animal Technology Co., Ltd.) were used as negative controls. The rats used in the present study were all male. A total of 20 13-week-old SHRs (Beijing Vital River Laboratory Animal Technology Co., Ltd.) (weight, 200±20 g) were equally divided into the following two groups: The SHR group and the SHR + allisartan group, based on whether allisartan treatment (240 mg/tablet; Shenzhen Salubris Pharmaceuticals Co., Ltd.) was administered or not. All animals were housed under a 12-h light/dark cycle, and were provided with free access to tap water and chow feed in a laboratory environment (temperature, 23.0±1.0˚C; humidity, 55.0±5.0%). After acclimation for 1 week in an on-site facility, the SHR + allisartan group of rats was orally administered allisartan in 1 ml distilled water for 34 weeks. The SHR and WKY control groups were orally administered 1 ml distilled water for 34 weeks. No animals died before the final timepoint.

The dose of allisartan was determined using the body surface area conversion coefficient (22,23). Briefly, the human equivalent dose for the daily oral administration of 240 mg allisartan to a person weighing 60 kg is 4 mg/kg/day. According to the literature, the surface area conversion coefficient for rats corresponding to a human weighing 60 kg is 0.16, expressed as human dose in mg/kg=0.16 x animal dose in mg/kg. Consequently, the dose of allisartan administered to rats was 25 mg/kg/day.

At the end of the experiment, the rats were anesthetized via intraperitoneal injection of 5% chloral hydrate (300 mg/kg), and the heart tissue was removed from the rats once they were fully anesthetized. All animal experimental procedures were carried out in accordance with the Guide for the Care and Use of Laboratory Animals of the National Institutes of Health (24), and the Animal Research: Reporting *In Vivo* Experiments: The ARRIVE Guidelines (25) and the present study was approved by the Animal Ethics Committee of Tianjin Union Medical Center (approval no. 2022C07; Tianjin, China). The humane endpoint of this study was: Weight loss ≥20% (compared with the original weight of the rat).

Measurement of blood pressure. The rats were kept in a conscious and immobilized state to ensure blood pressure sensors were fixed to the tail, and were maintained at a suitable temperature (30-35˚C) and level of awareness for the duration of the experiment. The systolic and diastolic blood pressure levels of the rats in each group were monitored every 2 weeks, using a blood pressure analysis system (CODA-HT8; Kent Scientific Corp), from 14-weeks-old to 48-weeks-old.

Echocardiography. Echocardiography was performed on rats at 14, 28 and 48-weeks-old. The rats were anesthetized via intraperitoneal injection of 5% chloral hydrate (300 mg/kg). The following indicators were measured: Interventricular septum end-diastolic thickness and left ventricular posterior wall thickness in diastole. Left ventricle mass and ejection fraction (EF, %) were also calculated. The measurements were performed using an ultra-high resolution small animal ultrasound scanner (Vevo2100; FUJIFILM VisualSonics), guided by transthoracic two-dimensional M-mode echocardiography.

Morphological and histological analysis. At the end of the experiment, the rats were anesthetized via intraperitoneal injection of 5% chloral hydrate (300 mg/kg), and the heart tissue was removed after the rats were fully anesthetized. Subsequently, the heart tissue was washed with PBS before being fixed in 4% paraformaldehyde for 48 h, at 4˚C. Subsequently, sections were dehydrated in an ascending alcohol series and embedded

in paraffin. Paraffin-embedded sections (3-5 μm) were then stained with Masson's trichrome and wheat germ agglutinin (WGA). Masson's trichrome staining was performed using the Masson's Trichrome Stain Kit (cat. no. G1340; Beijing Solarbio Science & Technology Co., Ltd.) according to the manufacturer's protocol. Collagen volume fraction and cell cross-sectional area (CSA) were used to evaluate the degree of cardiac fibrosis and cell hypertrophy, respectively. WGA staining was performed by incubating the slides with WGA-FITC-labeled antibodies (1:200; cat. no. L4895; MilliporeSigma) for 30 min at 23-26˚C, followed by staining the nuclei with DAPI for 5 min at 23-26˚C. For each analysis, six fields were randomly selected from each sample under a fluorescence microscope (ECLIPSE C1; Nikon Corporation).

Transcriptome and proteome analyses. The transcriptome of the SHR group vs. the WKY group, and the SHR + allisartan group vs. the SHR group were analyzed by RNA-sequencing (RNA-seq) using TruSeq Stranded mRNA LT Sample Prep Kit (cat. no. RS-122-2101; Illumina, Inc.) and the Illumina HiSeq™ 2500 sequencing platform (Illumina, Inc.). Total RNA was extracted from heart tissue using the mirVana miRNA Isolation Kit (cat. no. Ambion-1561; Thermo Fisher Scientific, Inc.) and integrity was evaluated using the Agilent 2100 Bioanalyzer (Agilent Technologies, Inc.). The samples with RNA Integrity Number ≥7 were subjected to the subsequent analysis.The concentration of the library was measured using the Qubit dsDNA Assay Kit (cat. no. Q328520; Thermo Fisher Scientific, Inc.), and the loading concentration of the final library was 20 pM. Subsequently, these libraries were sequenced on the Illumina HiSeq™ 2500 sequencing platform and 125 bp/150 bp paired-end reads were generated. Differentially expressed genes (DEGs) were identified using DESeq R package (Version 1.18.0) (26) with specific criteria for significant differential expression. For determining significant differential expression, the threshold values were set as P<0.05 and |log2 FC| >1.

The proteome of the SHR + allisartan group vs. the SHR group was analyzed by tandem mass tag (TMT) technology. Total protein was extracted from heart tissue using SDS lysis buffer (Beyotime Institute of Biotechnology) with 1 mM PMSF (Amresco, LLC), and a portion was used for protein concentration determination using the BCA Protein Assay Kits (cat. no. A55864; Thermo Fisher Scientific, Inc.) and 12% SDS-PAGE. After protein quantification, 100 μg each sample underwent trypsin digestion and TMT labeling, and liquid chromatography tandem mass spectrometry (LC-MS/MS; TripleTOF 6600; SCIEX) was performed on the samples for analysis and data analysis. For LC-MS/MS, the spray voltage was set to 2.4 kV, curtain gas pressure to 40 PSI, nebulizer gas pressure to 12 PSI, and heater temperature to 150˚C. Mass spectrometry scanning was performed in Information Dependent Analysis (IDA) mode. The first-level full scan range was m/z 350-1,500 with a scan time of 250 msec. Under each IDA cycle, 42 precursor ions with charges +2 to +4 and a single second count greater than 260 were selected for second-level fragmentation scans. The second-level scan range was m/z 100-1,500 with a scan time of 50 msec. Collision energy was set for collision-induced dissociation for all precursor ions. Dynamic exclusion was set to 14 sec. The experimental data were analyzed using ProteinPilot 5.0 (SCIEX) based on the Uniprot rat database (https://www.uniprot.org/taxonomy/10116). The results were screened according to the standard of Score Sequest HT >0 and unique peptide ≥1, while excluding the blank value. Differentially expressed proteins were selected based on the standard of FC >1.2 or FC <5/6 and P<0.05 for significantly differential expression. Subsequently, functional analysis was performed on the differentially expressed proteins, including Gene Ontology (GO) analysis, Kyoto Encyclopedia of Genes and Genomes (KEGG) pathway analysis and protein-protein interaction (PPI) analysis. GO, KEGG and PPI analyses were all performed on the Omicsbean cloud platform (http://www.omicsbean.cn/). Finally, all differentially expressed proteins and DEGs were compared by combined transcriptome and proteome analysis.

Immunofluorescence staining and TUNEL assay. Antigen retrieval of the aforementioned paraffin-embedded heart tissue sections (5 μm) was conducted by heating at a temperature of 90-95˚C with EDTA (pH 8.0; cat. no. G1206; Wuhan Servicebio Technology Co., Ltd.). Deparaffinization and rehydration were then achieved by incubating sections in xylene twice, each time for 15-20 min. Subsequently, dehydration was carried out in pure ethanol twice, each time for 10 min, followed by dehydration in a gradient of ethanol concentrations (95, 90, 80 and 70% ethanol) for 5 min each. Sections were then washed in distilled water and blocking was performed with 3% BSA (cat. no. GC305010; Wuhan Servicebio Technology Co., Ltd.) for 30 min at 23-26˚C. Subsequently, a primary antibody against Nrf2 (1:1,000; cat. no. GB113808-100; Wuhan Servicebio Technology Co., Ltd.) was added and incubated overnight at 4˚C. After washing the sections with PBS three times, a secondary antibody (Cy3-conjugated Goat Anti-Rabbit IgG; 1:300; cat. no. GB21303; Wuhan Servicebio Technology Co., Ltd.) was added and incubated at room temperature for 50 min in the dark.

TUNEL staining was performed using the FITC TUNEL Cell Apoptosis Detection Kit (Wuhan Servicebio Technology Co., Ltd.), according to the manufacturer's protocol. After washing the sections with PBS three times, DAPI staining solution was added and incubated at room temperature for 10 min.

For each analysis, six fields were randomly selected from each sample under a fluorescence microscope(ECLIPSE C1; Nikon Corporation). To calculate the nuclear ratio of Nrf2, the nuclear Nrf2 fluorescence intensity was divided by the total Nrf2 fluorescence intensity. To calculate the apoptotic index, the number of TUNEL-positive cells was divided by the number of DAPI-positive cells.

Western blotting. Proteins were extracted from myocardial tissue using the total protein extraction kit (cat. no. KGB5303-100; Nanjing KeyGen Biotech Co., Ltd.) according to the manufacturer's protocol. The protein concentration was determined using the BCA method (Beijing Solarbio Science & Technology Co., Ltd.). Subsequently, 30 μg proteins were separated by SDS-PAGE on 10% gels using the TGX stain-free kit (Bio-Rad Laboratories, Inc.) and were transferred to a polyvinylidene difluoride (PVDF)

membrane (GE Healthcare). The PVDF membrane was then blocked in 5% non-fat milk in TBS-0.1% Tween (TBST) at room temperature for ~1 h. The following primary antibodies: Pro-collagen I (cat. no. bs-0578R; Bioss; 1:500); collagen III (cat. no. bs-0948R; Bioss; 1:500); phosphorylated (p)-AKT (cat. no. 4060; Ser473; Cell Signaling Technology, Inc.; 1:1,000); AKT (cat. no. 9272; Cell Signaling Technology, Inc.; 1:1,000); p-PI3K (cat. no. 17366; Tyr458; Cell Signaling Technology, Inc.; 1:1,000); PI3K (cat. no. 4255; Cell Signaling Technology, Inc.; 1:1,000) and GAPDH (cat. no. AC001; Abclonal Biotech Co., Ltd.; 1:1,000), were added and incubated overnight at 4˚C. The PVDF membrane was then washed three times for 5 min with TBST, followed by incubation with the corresponding HRP-labeled secondary antibody (cat. no. bs-80295G-HRP; Bioss; 1:5,000) at room temperature for 2 h. Finally, the PVDF membrane was washed three times for 5 min with TBST, and the blot was visualized using the Gel Doc XR system (Bio-Rad Laboratories, Inc.) and Immobilon ECL Ultra Western HRP Substrate (cat. no. WBULS0100; MilliporeSigma). Image J (version 1.80; National Institutes of Health) was used to semi-quantify the protein expression.

Reverse transcription-quantitative PCR (RT-qPCR). RNA was extracted from myocardial tissue using TRIzol reagent (Invitrogen; Thermo Fisher Scientific, Inc.) according to the manufacturer's protocol. The concentration of the total RNA was measured using a Biophotometer Plus (Eppendorf UK Limited) and equal amounts of total RNA were reverse transcribed into cDNA using the Transcriptor First Strand cDNA Synthesis Kit according to the manufacturer's protocol (Roche Diagnostics). qPCR was performed as follows: Initial denaturation at 95˚C for 30 sec, followed by 40 cycles at 94˚C for 5 sec and 60˚C for 30 sec, using the Fast Start Universal SYBR Green Master Mix Kit (Roche Diagnostics) with specific primers for Col1a1, Col3a1 and Gapdh on a Step-One Real-Time PCR system (Bio-Rad Laboratories, Inc.). The relative expression levels of Col1a1 and Col3a1 in the different groups were normalized to the expression levels of the reference gene Gapdh. The mRNA expression levels was determined using the $2^{-\Delta\Delta Cq}$ method (27). The primer (5'-3') sequences used were as follows: Col1a1, forward ACGCAT GGCCAAGAAGACATC, reverse TTTGCATAGCACGCC ATCG; Col3a1, forward CAGCTGGCCTTCCTCAGACTT, reverse GCTGTTTTTGCAGTGGTATGTAATGT; Gapdh, forward CAGCAAGGATACTGAGAGCAAGAG, reverse GGATGGAATTGTGAGGGAGATG.

Statistical analysis. Statistical analysis was conducted using SPSS 22.0 software (IBM Corp.). All experimental data are presented as the mean ± standard deviation. Differences between groups were analyzed by one-way ANOVA, followed by the LSD-t post-hoc multiple comparisons test. Differences between groups and ages were analyzed by mixed ANOVA and Tukey's HSD post-hoc test. $P<0.05$ was considered to indicate a statistically significant difference.

Results

Allisartan reduces blood pressure, attenuates cardiac remodeling and improves cardiac function. Compared with those in the WKY group, both systolic and diastolic blood pressure levels in the SHR group were significantly increased during weeks 14-48 (Fig. 1A). Compared with in the SHR group, treatment with allisartan for 2 weeks in the SHR + allisartan group effectively controlled both systolic and diastolic blood pressure levels in rats during weeks 16-48 (Fig. 1A). At 48 weeks of age, there were no significant differences in body weight or heart weight among the three groups of rats (Fig. 1B). However, compared with that in the WKY group, the heart weight/body weight ratio was significantly increased in the SHR group, and it was significantly decreased in the SHR + allisartan group compared with that in the SHR group (Fig. 1B).

Echocardiography was performed at three time points (14, 28 and 48 weeks) to evaluate the effects of hypertension and allisartan on cardiac remodeling and function in rats. The results of echocardiography (Fig. 1C and D) showed that LVPWd, IVSd and left ventricle mass increased, and ventricular wall thickening appeared in the SHR group at 28 weeks of age, accompanied by a decrease in EF. With the passage of time, EF continued to decline until the SHRs reached 48 weeks of age. Allisartan could relieve cardiac remodeling and improve heart function in SHRs at 28 weeks, and this cardioprotective effect persisted until week 48.

Allisartan alleviates cardiomyocyte hypertrophy and cardiac fibrosis. The present study further evaluated the morphological changes in myocardial tissue. WGA staining was used to observe cardiomyocyte volume. Compared with that in the WKY group, the CSA of cardiomyocytes in the SHR group was significantly increased, indicating cardiomyocyte hypertrophy; however, allisartan was able to reverse this cardiomyocyte hypertrophy (Fig. 2A and B). Subsequently, Masson staining was used to observe the degree of myocardial fibrosis. At 48 weeks, the myocardial tissue of SHRs showed significant collagen fiber deposition, whereas allisartan effectively reduced the degree of myocardial fibrosis (Fig. 2C and D). Consistent with these findings, the expression levels of myocardial tissue fibrotic markers, pro-collagen I and collagen III, were significantly increased in the SHR group, whereas allisartan reduced their expression levels in the myocardial tissue of SHRs (Fig. 2E and F).

Effects of allisartan on the myocardial transcriptome and proteome. To further investigate the protective mechanism of allisartan in SHRs, RNA-seq was performed to compare DEGs between the SHR group and the WKY group, as well as between the SHR + allisartan group and the SHR group. The threshold for significant DEGs was set as FC >2 or FC <0.5 and $P<0.05$. The RNA-seq results showed that, compared with the WKY group, there were 677 upregulated genes and 258 downregulated genes in the SHR group (Fig. 3A). In addition, when compared with the SHR group, the SHR + allisartan group had 296 upregulated genes and 526 downregulated genes (Fig. 3A).

To exert their biological functions, the vast majority of mRNA molecules need to be translated into their corresponding proteins. The present study further compared the differentially expressed proteins between the SHR + allisartan group and the SHR group using TMT technology. Proteins

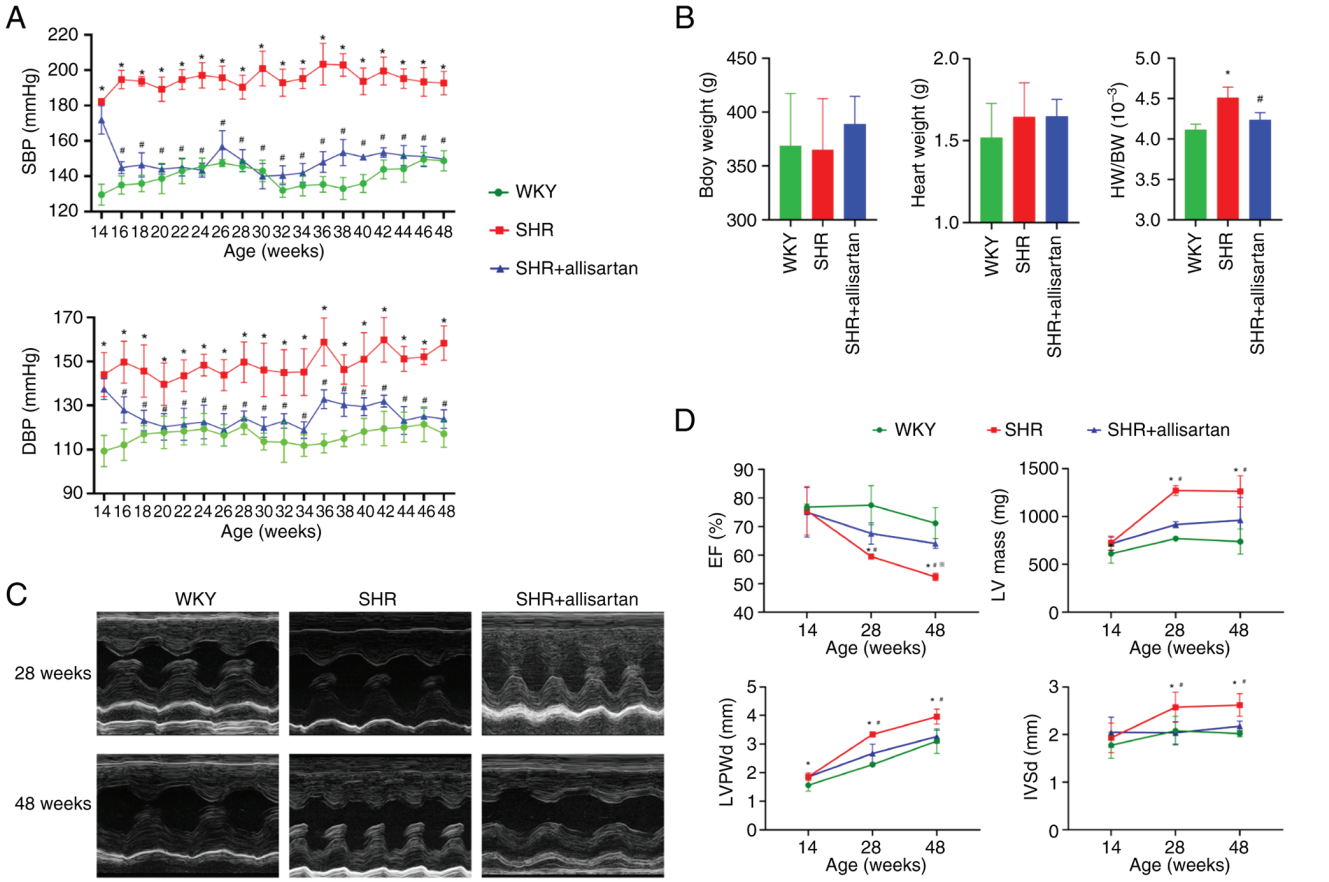

Figure 1. Allisartan reduces blood pressure, attenuates cardiac remodeling and improves cardiac function (A) SBP and DBP levels of rats aged 14-48 weeks. (B) BW, HW and HW/BW ratio of rats aged 48 weeks. *P<0.05 vs. WKY group; #P<0.05 vs. SHR group. (C) Representative images of echocardiography at 28 and 48 weeks. (D) EF (%), LV mass, LVPWd and IVSd measured by echocardiography. Differences between groups were analyzed by ANOVA and LSD-t post-hoc test, and differences between groups and ages were analyzed by mixed ANOVA and Tukey's HSD post-hoc test. Data are presented as the mean ± SD. *P<0.05 vs. WKY group at the same age; #P<0.05 vs. SHR group at the same age; □P<0.05 vs. SHR group at 28 weeks of age. BW, body weight; DBP, diastolic blood pressure; EF, ejection fraction; HW, heart weight; IVSd, interventricular septum end-diastolic thickness; LV, left ventricle; LVPWd, left ventricular posterior wall thickness in diastole; SBP, systolic blood pressure; SHR, spontaneously hypertensive rat.

with FC >1.2 or FC <5/6 and P<0.05 were considered significantly differentially expressed. The results showed that there were a total of 257 significantly differentially expressed proteins between the SHR + allisartan group and the SHR group, with 76 upregulated and 181 downregulated (Fig. 3B). Subsequently, functional analysis was performed on the differentially expressed proteins, including GO, KEGG pathway and PPI analyses. The results of the GO analysis indicated that differentially expressed proteins were mainly enriched in 'fibril organization', 'cytoplasm' and 'protein binding'. The top five pathways identified by KEGG pathway analysis were 'pentose phosphate pathway', 'fatty acid elongation', 'valine, leucine and isoleucine degradation', 'glutathione metabolism' and 'amino sugar and nucleotide sugar metabolism'. The PPI analysis revealed the possible interactions between the differentially expressed proteins involved in the aforementioned pathways. It was revealed that Gstm2, which is involved in glutathione metabolism, may interact with Eci1 and Gpx1 (Fig. 3B).

Finally, through the combined transcriptome and proteome analysis, 10 genes that were upregulated at both the mRNA and protein levels, and 21 genes that were downregulated at both the mRNA and protein levels were identified (Fig. 3C; Table I). Among these 10 commonly upregulated genes was GSTM2, which was significantly upregulated at both the mRNA (fold change 2.123403, P<0.05) and protein (fold change 1.412545235, P<0.05) levels. This protein is an important member of the glutathione metabolism pathway, which serves a role in detoxifying ROS (28).

Allisartan reduces cardiomyocyte apoptosis and activates the PI3K-AKT-Nrf2 signaling pathway. It is well known that a large amount of ROS can induce cell apoptosis. The present study assessed the level of cell apoptosis by TUNEL staining, and the results showed a significant increase in cardiomyocyte apoptosis in the SHR group compared with that in the WKY group, whereas allisartan was able to reduce cardiomyocyte apoptosis in SHRs (Fig. 4A).

The present study further investigated the PI3K-AKT signaling pathway. Western blotting results showed that the phosphorylation levels of PI3K and AKT were decreased in the cardiomyocytes of SHRs, indicating that the PI3K-AKT signaling pathway was inhibited (Fig. 4B). However, allisartan was able to restore the phosphorylation levels of PI3K and AKT in the cardiomyocytes of SHRs, thus activating the PI3K-AKT signaling pathway.

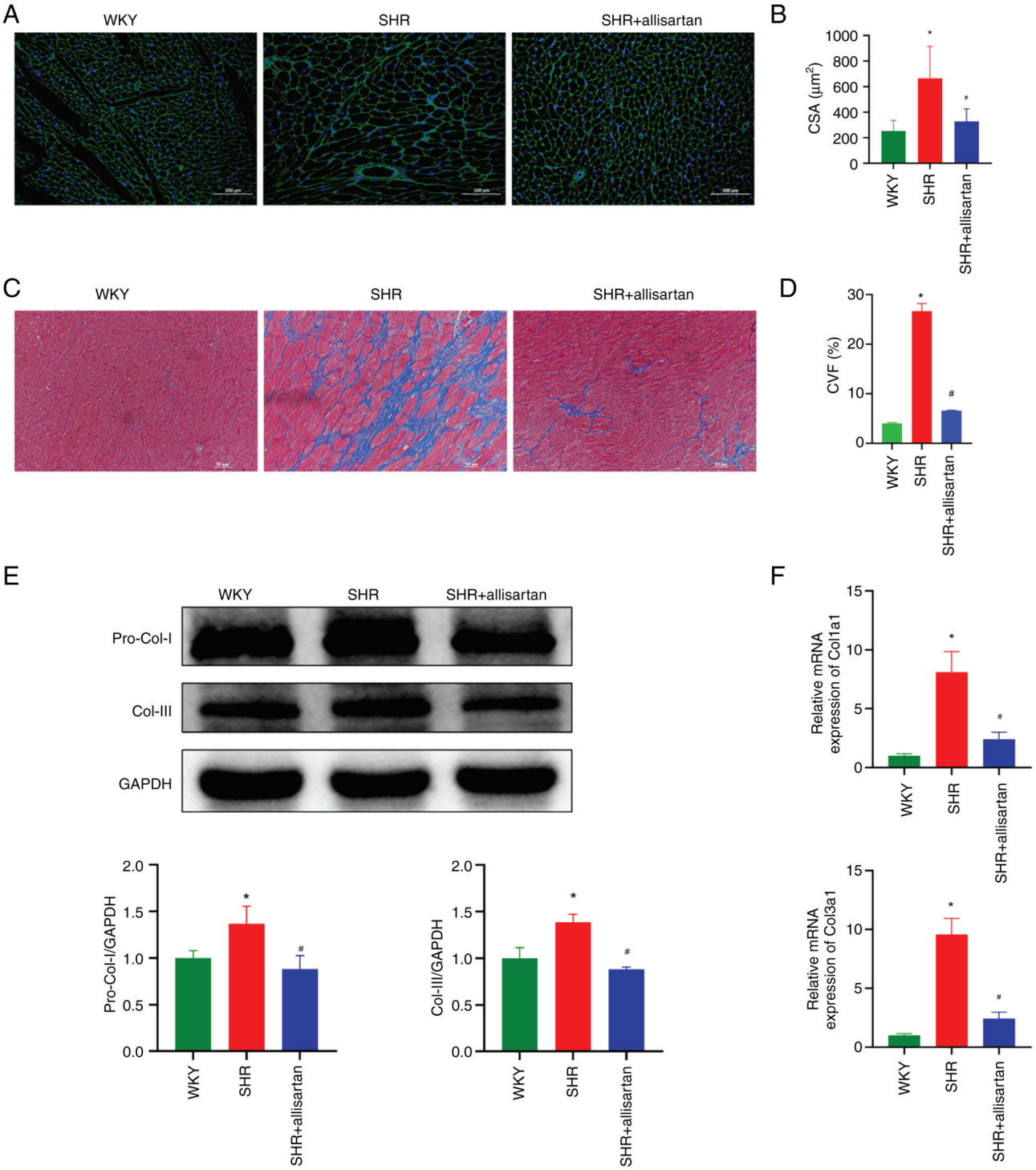

Figure 2. Allisartan alleviates cardiomyocyte hypertrophy and cardiac fibrosis. (A) Representative images of WGA staining and (B) cell CSA semi-quantification. Scale bar, 100 μm. (C) Representative images of Masson staining and (D) CVF semi-quantification. Scale bar, 50 μm. (E) Western blotting was used to detect the expression levels of Pro-Col-I and Col-III. (F) Reverse transcription-quantitative PCR analysis was used to detect the mRNA expression levels of Col1a1and Col3a1. Differences between groups were analyzed by ANOVA and LSD-t post-hoc test. Data are presented as the mean ± SD. *P<0.05 vs. WKY group; $^{\#}$P<0.05 vs. SHR group. Col, collagen; CSA, cross-sectional area; CVF, collagen volume fraction; SHR, spontaneously hypertensive rat.

Through immunofluorescence co-localization, the nuclear Nrf2 ratio was analyzed. The results showed that Nrf2 in the cardiomyocytes of SHRs was mainly distributed in the cytoplasm and did not enter the nucleus to function as a transcription factor; by contrast, allisartan significantly increased the nuclear entry of Nrf2 in the cardiomyocytes of SHRs (Fig. 4C).

Discussion

The present study evaluated the effects of allisartan on lowering blood pressure, and improving hypertension-related cardiac remodeling and cardiac dysfunction in SHRs. In addition, the impact of allisartan on the transcriptome and proteome of SHRs was assessed, and it was shown to have significant

Table I. Genes that are significantly upregulated or downregulated at the mRNA and protein levels in the combined transcriptome and proteome analysis of SHR + allisartan vs. SHR.

A, SHR + allisartan vs. SHR upregulated genes and proteins

Gene	Protein
Myh6	G3V885
Atp1a2	P06686
Acsf2	Q499N5
Acot2	O55171
Gstm2	P08010
Lsamp	Q62813
S100a9	P35467
S100a8	P50115
S100a9	A0A0H2UHJ1
Tmod4	D3ZSG3

B, SHR + allisartan vs. SHR downregulated genes and proteins

Gene	Protein
Acta1	P68136
Anxa1	P07150
Bgn	P47853
Csrp2	G3V9V9
Flnc	D3ZHA0
Gda	Q9JKB7
Hopx	Q78ZR5
LOC100909761	M0RCF7
Maoa	G3V9Z3
Mfap5	D3ZJB1
Ncam1	P13596
Nppa	P01161
Pgm3	D3ZFX4
Postn	A0A097BW25
Sypl2	D4A6M0
Tgm2	Q9WVJ6
Thbs4	P49744
Tor3a	Q5M936
Uchl1	Q00981
Xirp2	F1LMC2
Xirp2	Q71LX6

effects on GSTM2 and its involvement in glutathione metabolism. GSTM2 was significantly upregulated by allisartan at both the mRNA and protein levels. Thus, the ability of allisartan to alleviate cardiac remodeling, improve cardiac dysfunction and prevent cardiomyocyte apoptosis may be related to the upregulation of GSTM2 expression. Moreover, the regulation of GSTM2 expression by allisartan may be associated with activation of the PI3K-AKT-Nrf2 signaling pathway. The findings of the present study are conclusive in male rats, whereas the potential impact of sex on the results should be explored in future research.

Hypertension is an important risk factor for CVD (29). Prolonged pressure overload can cause structural changes in the heart, leading to cardiac remodeling. The most obvious characteristics of hypertension-induced cardiac remodeling are ventricular hypertrophy and myocardial fibrosis. During the compensatory phase, ventricular hypertrophy increases heart mass and maintains myocardial contractility, which is beneficial to the heart in the early stages. However, if it exceeds a certain degree, the decompensated phase can cause a decrease in myocardial contractility, a decrease in diastolic function and even worsening heart failure (30,31). Ventricular hypertrophy reduces myocardial contractility and ejection ability, and coronary blood flow is insufficient to meet the oxygen demand of the heart itself, which can cause myocardial ischemia and myocardial cell damage (32,33). After myocardial injury, the heart muscle cells no longer have regenerative ability; therefore, fibroblasts repair the heart by increasing ECM components, forming scar tissue (33). At this point, fibroblasts can secrete large amounts of type I and III collagen, the latter of which deposits in the ECM, causing diffuse myocardial fibrosis, reducing heart diastolic function and compliance (34,35).

SHRs are widely used in research related to hypertension and target organ damage caused by hypertension (36-39). In the present study, the blood pressure of SHRs was significantly increased and, at 28 weeks, echocardiography showed signs of cardiac remodeling, characterized by thickening of the ventricular wall, an increase in left ventricle mass and a decrease in EF. As the disease progressed, heart function further deteriorated at 48 weeks, consistent with the entire process of the occurrence and development of hypertensive heart disease. The morphological changes in the myocardial tissue of SHRs were manifested by cardiomyocyte hypertrophy, collagen deposition and increased expression of myocardial fibrosis markers, indicating typical cardiac remodeling (40). Treatment with allisartan effectively controlled the blood pressure of SHRs and, by 28 weeks, cardiac remodeling and functional impairment were improved. Furthermore, this cardioprotective effect continued with the administration of allisartan.

The protective effect of antihypertensive drugs on the heart is not only due to reducing blood pressure and decreasing cardiac load. It is well known that ARB/Ang-converting enzyme inhibitor drugs improve cardiac remodeling by inhibiting the RAAS and improving overactivation of the neuroendocrine system (41,42). However, the deeper mechanisms are still not fully understood. Currently, research has shown that the cardioprotective effects of ARB antihypertensive drugs, such as candesartan, are partly independent of blood pressure (43). ZnCand, a coordination complex synthesized between the ARB candesartan and Zn(II), can exert cardioprotective effects by suppressing NOX2 to inhibit oxidative stress and restore redox homeostasis (44). Losartan regulates macrophage polarization via the TLR4/NF-κB/MAPK pathway to alleviate sepsis-induced myocardial injury (45). As a new type of ARB drug, allisartan not only effectively controls blood pressure, but it has also been shown to exert protective effects on the heart, kidneys and large arteries in hypertensive animals. Additionally, allisartan has lower toxicity than losartan (46). Clinical studies have also confirmed the protective effects of

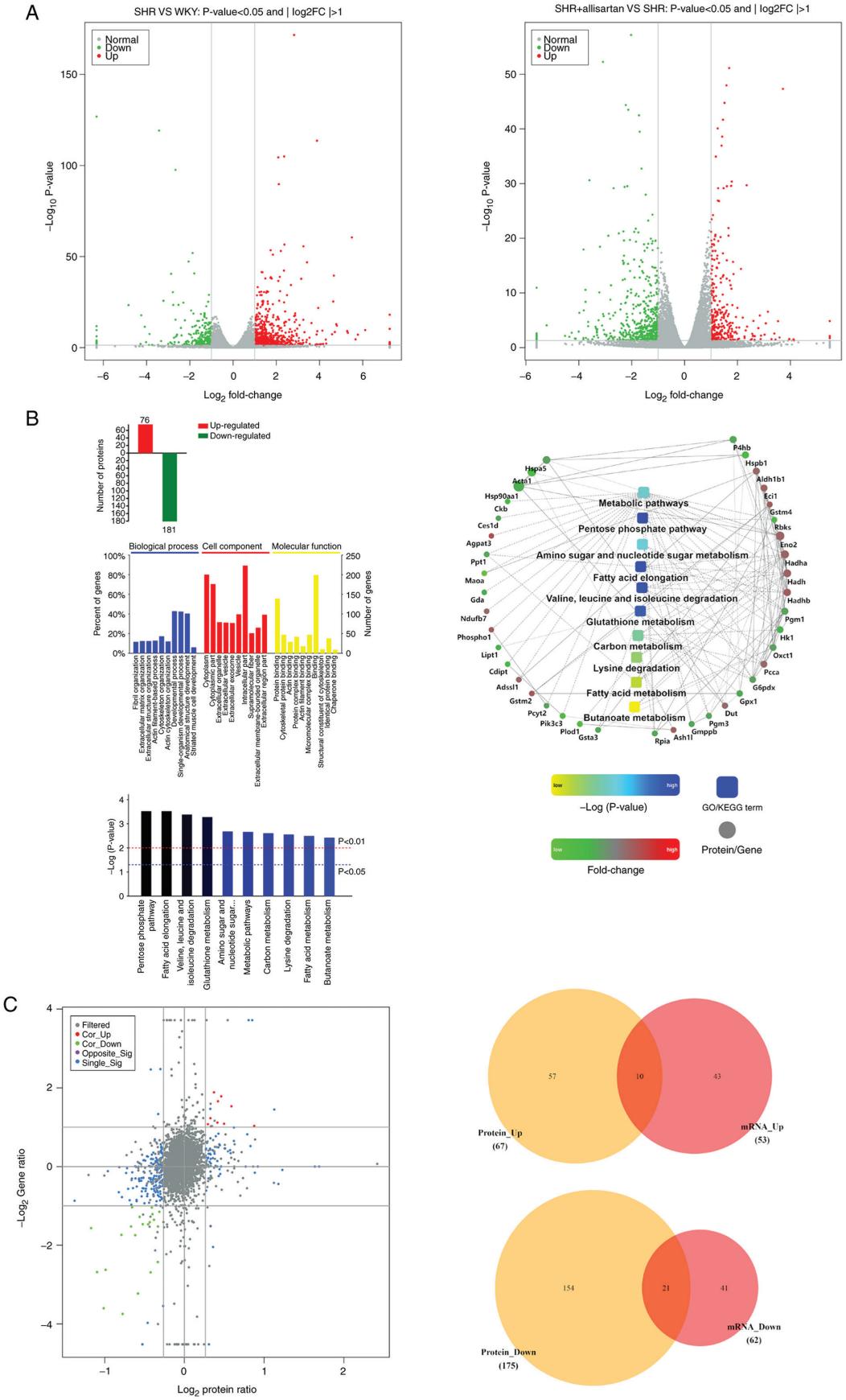

Figure 3. Effects of allisartan on the myocardial transcriptome and proteome. (A) Volcano plots illustrate differential gene expression in the transcriptome between the SHR and WKY groups, as well as between the SHR + allisartan and SHR groups. To determine significantly differentially expressed genes, the threshold values were set as P<0.05 and FC >2 or FC <0.5. (B) Differential protein expression between the SHR + allisartan and SHR groups; significantly differentially expressed proteins were selected based on the standard of FC >1.2 or FC <5/6 and P<0.05. The results of KEGG pathway and protein-protein interaction analyses are shown. (C) Results of integrated transcriptome and proteome analysis of SHR + allisartan vs. SHR. FC, fold change; GO, Gene Ontology; KEGG, Kyoto Encyclopedia of Genes and Genomes; SHR, spontaneously hypertensive rat.

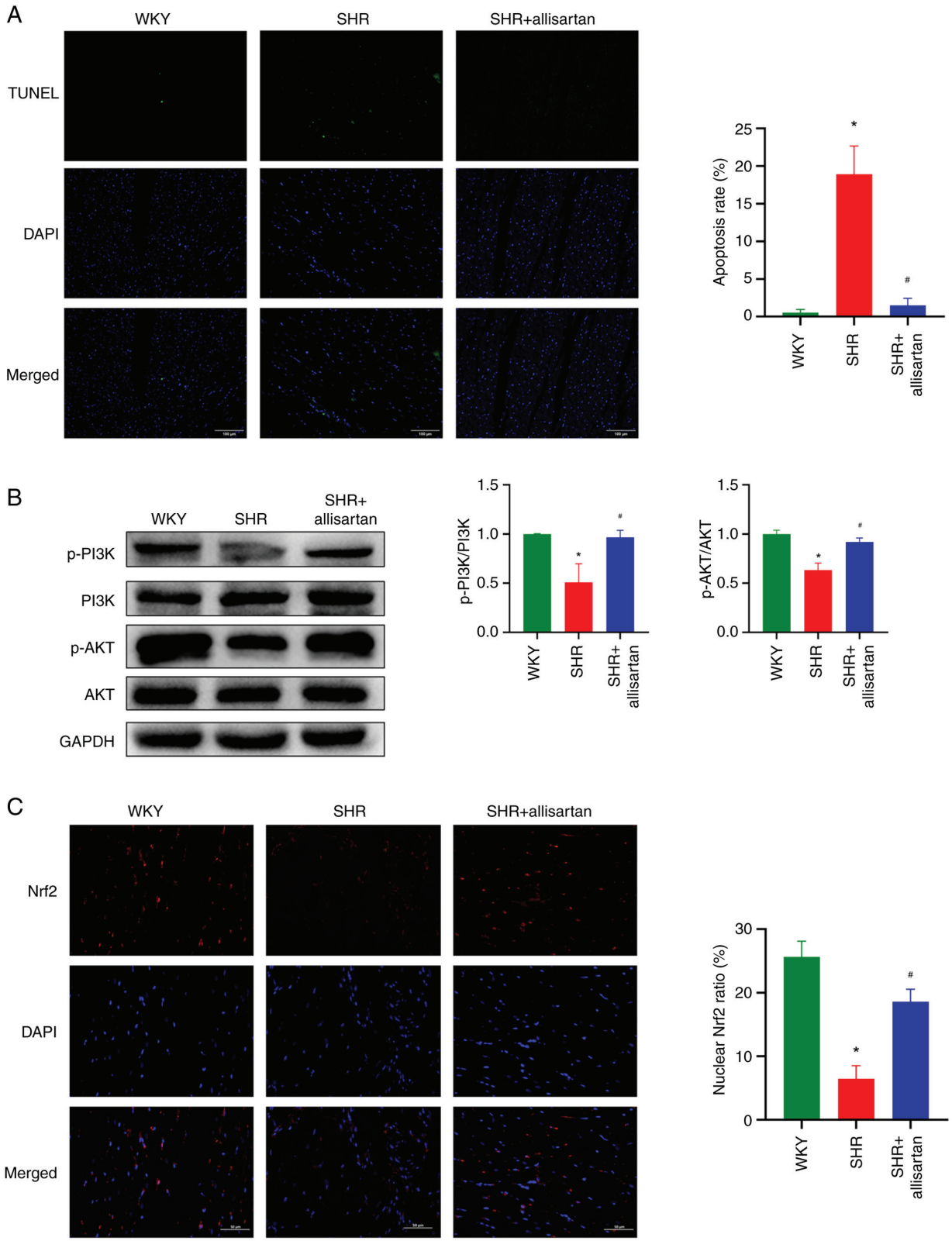

Figure 4. Allisartan reduces cardiomyocyte apoptosis and activates the PI3K-AKT-Nrf2 signaling pathway. (A) Representative images of DNA fragmentation as assessed by TUNEL assay and DAPI staining. Scale bar, 100 μm. (B) Western blotting was used to detect the expression levels of p-AKT, AKT, p-PI3K and PI3K. (C) Representative images of Nrf2 nuclear translocation detected by immunofluorescence. Scale bar, 50 μm. Differences between groups were analyzed by ANOVA and LSD-t post-hoc test. Data are presented as the mean ± SD. *P<0.05 vs. WKY group; $^{\#}$P<0.05 vs. SHR group. p-, phosphorylated; SHR, spontaneously hypertensive rat.

allisartan on the heart, kidneys and large arteries of patients with hypertension (47,48). Furthermore, allisartan can reduce the risk of stroke-related death in hypertensive rats, which may be related to its inhibition of NAD(P)H oxidase expression to alleviate oxidative stress (4). Allisartan can also activate SIRT1/Nrf2, inhibit NF-κB, and alleviate oxidative stress

and inflammation in diabetic rats (6), and it can regulate voltage-gated potassium channels in hypertensive rats to alleviate cardiac and vascular remodeling (8,9).

In the present study, high-throughput sequencing technology was used to analyze the transcriptome and proteome of rat hearts to further elucidate the protective effects of allisartan on hypertension-induced cardiac injury. Both hypertension and allisartan had significant effects on the rat cardiac transcriptome. According to the pathway analysis, allisartan mainly affected the 'pentose phosphate pathway', 'fatty acid elongation', 'valine, leucine and isoleucine degradation', 'glutathione metabolism' and 'amino sugar and nucleotide sugar metabolism' pathways. Through transcriptome and proteome analyses, it was identified that the mRNA and protein expression levels of GSTM2 were significantly upregulated by allisartan treatment. Glutathione is an important member of the endogenous antioxidant defense system (49), and GSTM2 is one of the important members involved in the metabolism of glutathione. Research has found that cardiac remodeling in SHRs is related to impaired antioxidant stress due to a significant decrease in GSTM2 expression (10). Another study suggested that overexpression of GSTM2 can inhibit oxidative stress-induced renal cell apoptosis and inflammation (28). Therefore, it was hypothesized that the cardioprotective effect of allisartan in SHRs may be related to its upregulation of GSTM2 expression, enhancing the ability to clear ROS, reducing oxidative stress damage and alleviating oxidative stress-induced apoptosis. In addition to its role as an antioxidant, studies have also reported that GSTM2 can restore cellular and mitochondrial autophagy flux to exert a protective effect on cells (13,14), and the C-terminal domain of GSTM2 can inhibit the binding of the cardiac ryanodine receptor to exert an anti-arrhythmic effect (15). Small extracellular vesicles rich in GSTM2 have been shown to ameliorate senescence-related tissue damage (16). In addition, a recent study showed that GSTM2 in the liver can block the N-terminal dimerization and phosphorylation of ASK1 to inhibit the ASK1/JNK/p38 signaling pathway, exerting anti-inflammatory and anti-steatotic effects (50). Whether GSTM2 serves a broader role in the myocardial tissue of SHRs remains to be further studied; however, based on the results of the present study, it may be hypothesized that allisartan enhances antioxidant stress and reduces myocardial cell apoptosis by upregulating GSTM2 expression in myocardial tissue.

The present study subsequently conducted a preliminary experiment on the potential pathways by which allisartan upregulates GSTM2 expression. The results of the present study showed that allisartan activates the PI3K-AKT-Nrf2 signaling pathway in the myocardial tissue of SHRs. Nrf2 is involved in redox balance, and it upregulates downstream targets, such as SOD, CAT, HO-1 and NQO1, through nuclear translocation, promoting antioxidant enzyme activity and improving oxidative damage (51). The expression of GSTM2 has been reported to be significantly decreased in the liver of $Nrf2^{-/-}$ mice (52). Astaxanthin and omega-3 fatty acids can upregulate downstream target genes NQO1, HO-1 and GSTM2 against oxidative stress through the Nrf2-ARE pathway (53). Furthermore, nicotinamide mononucleotide upregulates the expression of antioxidant genes Gstm1, Gstm2 and Mgst1 by promoting the expression and nuclear translocation of Nrf2, and regulates the glutathione metabolism pathway to improve silica-induced lung injury in mice (54). A previous study also showed that the PI3K/AKT pathway mediates Nrf2 activation in L02 hepatocytes (55). Additionally, anthocyanins have been shown to mitigate oxidative stress, neurodegeneration and memory impairment in a mouse model of Alzheimer's disease through the PI3K/AKT/Nrf2/HO-1 pathway (56). Alongside the present findings, it may be hypothesized that upregulation of GSTM2 by allisartan is at least partially mediated through the PI3K-AKT-Nrf2 signaling pathway.

In conclusion, the present study identified that allisartan can effectively control blood pressure in SHRs, and can improve cardiac remodeling and cardiac dysfunction. Transcriptome and proteome analyses revealed that allisartan upregulated the expression levels of GSTM2 in the myocardial tissue of SHRs, and markedly affected glutathione metabolism. The cardioprotective effect of allisartan may be exerted through activation of the PI3K-AKT-Nrf2 signaling pathway to upregulate the expression of GSTM2, thus reducing the apoptosis of myocardial cells in SHRs.

Acknowledgements

Not applicable.

Funding

This study was supported by the following projects: The Project of Tianjin Municipal Health Commission on TCM (grant no. 2021028), the Tianjin Health Research Project (grant no. TJWJ2021QN019), the National Natural Science Foundation of China (grant no. 82100388) and the Project of the Science and Technology Development Fund of Tianjin Education Commission for Higher Education (grant no. 2020KJ197).

Availability of data and materials

The transcriptome data generated in the present study may be found in the Gene Expression Omnibus under accession number GSE254800 or at the following URL: https://www.ncbi.nlm.nih.gov/geo/query/acc.cgi?acc=GSE254800. The proteome data generated in the present study may be found in the PRIDE under accession number PXD048882 or at the following URL: http://www.ebi.ac.uk/pride/archive/projects/PXD048882. The other data generated in the present study may be requested from the corresponding author.

Authors' contributions

HW wrote the manuscript, and conceptualized the research methods and experimental design. YZ performed experiments and prepared the original draft. JY performed experiments and graphically visualized the experimental results. LW supervised the study, and conducted analysis and interpretation of data. XQ reviewed and edited the manuscript, and conducted analysis and interpretation of data. All authors read and approved the final manuscript. XQ and HW confirm the authenticity of all the raw data.

Ethics approval and consent to participate

The animal experiments in the present study were approved by the Animal Ethics Committee of Tianjin Union Medical Center (approval no. 2022C07).

Patient consent for publication

Not applicable.

Competing interests

The authors declare that they have no competing interests.

References

1. Dorans KS, Mills KT, Liu Y and He J: Trends in prevalence and control of hypertension according to the 2017 American College of Cardiology/American Heart Association (ACC/AHA) Guideline. J Am Heart Assoc 7: e008888, 2018.
2. Huang A, Li H, Zeng C, Chen W, Wei L, Liu Y and Qi X: Endogenous CCN5 Participates in Angiotensin II/TGF-β_1 networking of cardiac fibrosis in high angiotensin II-induced hypertensive heart failure. Front Pharmacol 11: 1235, 2020.
3. Testai L, Brancaleone V, Flori L, Montanaro R and Calderone V: Modulation of EndMT by hydrogen sulfide in the prevention of cardiovascular fibrosis. Antioxidants (Basel) 10: 910, 2021.
4. Ling QS, Zhang SL, Tian JS, Cheng MH, Liu AJ, Fu FH, Liu JG and Miao CY: Allisartan isoproxil reduces mortality of stroke-prone rats and protects against cerebrovascular, cardiac, and aortic damage. Acta Pharmacol Sin 42: 871-884, 2021.
5. Li X, Sun J, Guo Z, Zhong D and Chen X: Carboxylesterase 2 and intestine transporters contribute to the low bioavailability of Allisartan, a Prodrug of Exp3174 for hypertension treatment in humans. Drug Metab Dispos 47: 843-853, 2019.
6. Jin Q, Zhu Q, Wang K, Chen M and Li X: Allisartan isoproxil attenuates oxidative stress and inflammation through the SIRT1/Nrf2/NF-□B signalling pathway in diabetic cardiomyopathy rats. Mol Med Rep 23: 215, 2021.
7. Writing Committee Members; ACC/AHA Joint Committee Members: 2022 AHA/ACC/HFSA guideline for the management of heart failure. J Card Fail 28: e1-e167, 2022.
8. Zhang X, Zhao Z, Xu C, Zhao F and Yan Z: Allisartan ameliorates vascular remodeling through regulation of voltage-gated potassium channels in hypertensive rats. BMC Pharmacol Toxicol 22: 33, 2021.
9. Xu C, Zhao Z, Yuan W, Fengping Z, Zhiqiang Y and Xiaoqin Z: Effect of allisartan on blood pressure and left ventricular hypertrophy through Kv1.5 channels in hypertensive rats. Clin Exp Hypertens 44: 199-207, 2022.
10. Zhou SG, Wang P, Pi RB, Gao J, Fu JJ, Fang J, Qin J, Zhang HJ, Li RF, Chen SR, *et al*: Reduced expression of GSTM2 and increased oxidative stress in spontaneously hypertensive rat. Mol Cell Biochem 309: 99-107, 2008.
11. Sies H: Oxidative stress: A concept in redox biology and medicine. Redox Biol 4: 180-183, 2015.
12. van der Pol A, van Gilst WH, Voors AA and van der Meer P: Treating oxidative stress in heart failure: Past, present and future. Eur J Heart Fail 21: 425-435, 2019.
13. Huenchuguala S, Muñoz P, Zavala P, Villa M, Cuevas C, Ahumada U, Graumann R, Nore BF, Couve E, Mannervik B, *et al*: Glutathione transferase mu 2 protects glioblastoma cells against aminochrome toxicity by preventing autophagy and lysosome dysfunction. Autophagy 10: 618-630, 2014.
14. Huenchuguala S, Munoz P and Segura-Aguilar J: The importance of mitophagy in maintaining mitochondrial function in U373MG cells. Bafilomycin A1 restores aminochrome-induced mitochondrial damage. ACS Chem Neurosci 8: 2247-2253, 2017.
15. Hewawasam RP, Liu D, Casarotto MG, Board PG and Dulhunty AF: The GSTM2 C-Terminal Domain Depresses Contractility and Ca2+ transients in neonatal rat ventricular cardiomyocytes. PLoS One 11: e0162415, 2016.
16. Fafian-Labora JA, Rodriguez-Navarro JA and O'Loghlen A: Small extracellular vesicles have GST activity and ameliorate senescence-related tissue damage. Cell Metab 32: 71-86 e5, 2020.
17. Ndisang JF, Wu L, Zhao W and Wang R: Induction of heme oxygenase-1 and stimulation of cGMP production by hemin in aortic tissues from hypertensive rats. Blood 101: 3893-3900, 2003.
18. Cheng J, Gu W, Lan T, Deng J, Ni Z, Zhang Z, Hu Y, Sun X, Yang Y and Xu Q: Single-cell RNA sequencing reveals cell type- and artery type-specific vascular remodelling in male spontaneously hypertensive rats. Cardiovasc Res 117: 1202-1216, 2021.
19. Saha P, Mell B, Golonka RM, Bovilla VR, Abokor AA, Mei X, Yeoh BS, Doris PA, Gewirtz AT, Joe B, *et al*: Selective IgA deficiency in spontaneously hypertensive rats with gut dysbiosis. Hypertension 79: 2239-2249, 2022.
20. Okamoto K and Aoki K: Development of a strain of spontaneously hypertensive rats. Jpn Circ J 27: 282-293, 1963.
21. Kurtz TW and Morris RC Jr: Biological variability in Wistar-Kyoto rats. Implications for research with the spontaneously hypertensive rat. Hypertension 10: 127-131, 1987.
22. Reagan-Shaw S, Nihal M and Ahmad N: Dose translation from animal to human studies revisited. FASEB J 22: 659-661, 2008.
23. Liu W, Yu Z, Wang Z, Waubant EL, Zhai S and Benet LZ: Using an animal model to predict the effective human dose for oral multiple sclerosis drugs. Clin Transl Sci 16: 467-477, 2023.
24. National Research Council (US) Committee for the Update of the Guide for the Care and Use of Laboratory Animals: Guide for the Care and Use of Laboratory Animals, 8th edition. National Academies Press (US), Washington, DC, 2011.
25. Kilkenny C, Browne W, Cuthill IC, Emerson M and Altman DG; National Centre for the Replacement, Refinement and Reduction of Amimals in Research: Animal research: Reporting in vivo experiments-the ARRIVE guidelines. J Cereb Blood Flow Metab 31: 991-993, 2011.
26. Robinson MD, McCarthy DJ and Smyth GK: edgeR: A Bioconductor package for differential expression analysis of digital gene expression data. Bioinformatics 26: 139-140, 2010.
27. Livak KJ and Schmittgen TD: Analysis of relative gene expression data using real-time quantitative PCR and the 2(-Delta Delta C(T)) Method. Methods 25: 402-408, 2001.
28. Li Y, Yan M, Yang J, Raman I, Du Y, Min S, Fang X, Mohan C and Li QZ: Glutathione S-transferase Mu 2-transduced mesenchymal stem cells ameliorated anti-glomerular basement membrane antibody-induced glomerulonephritis by inhibiting oxidation and inflammation. Stem Cell Res Ther 5: 19, 2014.
29. Yildiz M, Oktay AA, Stewart MH, Milani RV, Ventura HO and Lavie CJ: Left ventricular hypertrophy and hypertension. Prog Cardiovasc Dis 63: 10-21, 2020.
30. Kemp CD and Conte JV: The pathophysiology of heart failure. Cardiovasc Pathol 21: 365-371, 2012.
31. Burchfield JS, Xie M and Hill JA: Pathological ventricular remodeling: Mechanisms: Part 1 of 2. Circulation 128: 388-400, 2013.
32. Shimizu I and Minamino T: Physiological and pathological cardiac hypertrophy. J Mol Cell Cardiol 97: 245-262, 2016.
33. Rosca MG, Tandler B and Hoppel CL: Mitochondria in cardiac hypertrophy and heart failure. J Mol Cell Cardiol 55: 31-41, 2013.
34. Fan W, Wang W, Mao X, Chu S, Feng J, Xiao D, Zhou J and Fan S: Elevated levels of p-Mnk1, p-eIF4E and p-p70S6K proteins are associated with tumor recurrence and poor prognosis in astrocytomas. J Neurooncol 131: 485-493, 2017.
35. Takeuchi CS, Kim BG, Blazey CM, Ma S, Johnson HW, Anand NK, Arcalas A, Baik TG, Buhr CA, Cannoy J, *et al*: Discovery of a novel class of highly potent, selective, ATP-competitive, and orally bioavailable inhibitors of the mammalian target of rapamycin (mTOR). J Med Chem 56: 2218-2234, 2013.
36. Bednarski TK, Duda MK and Dobrzyn P: Alterations of lipid metabolism in the heart in spontaneously hypertensive rats precedes left ventricular hypertrophy and cardiac dysfunction. Cells 11: 3032, 2022.
37. Guan J, Clermont AC, Pham LD, Ustunkaya T, Revenko AS, MacLeod AR, Feener EP and Simão F: Plasma kallikrein contributes to intracerebral hemorrhage and hypertension in stroke-prone spontaneously hypertensive rats. Transl Stroke Res 13: 287-299, 2022.
38. Luo M, Luo S, Xue Y, Chang Q, Yang H, Dong W, Zhang T and Cao S: Aerobic exercise inhibits renal EMT by promoting irisin expression in SHR. iScience 26: 105990, 2023.

39. Ye C, Geng Z, Zhang LL, Zheng F, Zhou YB, Zhu GQ and Xiong XQ: Chronic infusion of ELABELA alleviates vascular remodeling in spontaneously hypertensive rats via anti-inflammatory, anti-oxidative and anti-proliferative effects. Acta Pharmacol Sin 43: 2573-2584, 2022.
40. Qiu ZY, Yu WJ, Bai J and Lin QY: Blocking VCAM-1 ameliorates hypertensive cardiac remodeling by impeding macrophage infiltration. Front Pharmacol 13: 1058268, 2022.
41. Akazawa H, Yabumoto C, Yano M, Kudo-Sakamoto Y and Komuro I: ARB and cardioprotection. Cardiovasc Drugs Ther 27: 155-160, 2013.
42. Singh KD and Karnik SS: Angiotensin type 1 receptor blockers in heart failure. Curr Drug Targets 21: 125-131, 2020.
43. Takeuchi F, Liang YQ, Isono M, Ang MY, Mori K and Kato N: Transcriptomic response in the heart and kidney to different types of antihypertensive drug administration. Hypertension 79: 413-423, 2022.
44. Martinez VR, Martins Lima A, Stergiopulos N, Velez Rueda JO, Islas MS, Griera M, Calleros L, Rodriguez Puyol M, Jaquenod de Giusti C, Portiansky EL, *et al*: Effect of the structural modification of Candesartan with Zinc on hypertension and left ventricular hypertrophy. Eur J Pharmacol 946: 175654, 2023.
45. Chen XS, Wang SH, Liu CY, Gao YL, Meng XL, Wei W, Shou ST, Liu YC and Chai YF: Losartan attenuates sepsis-induced cardiomyopathy by regulating macrophage polarization via TLR4-mediated NF-κB and MAPK signaling. Pharmacol Res 185: 106473, 2022.
46. Wu MY, Ma XJ, Yang C, Tao X, Liu AJ, Su DF and Liu JG: Effects of allisartan, a new AT(1) receptor blocker, on blood pressure and end-organ damage in hypertensive animals. Acta Pharmacol Sin 30: 307-313, 2009.
47. Zhang G, Fan Y, Qiu Y, Zhou Z, Zhang J, Wang Z, Liu Y, Liu X and Tao J: Allisartan isoproxil improves endothelial function and vascular damage in patients with essential hypertension: A single-center, open-label, randomized controlled trial. Adv Ther 37: 3551-3561, 2020.
48. Zhang JQ, Yang GH, Zhou X, Liu JX, Shi R, Dong Y, Chen SB and Li YM: Effects of allisartan isoproxil on blood pressure and target organ injury in patients with mild to moderate essential hypertension. Medicine (Baltimore) 98: e14907, 2019.
49. Ma Q: Role of nrf2 in oxidative stress and toxicity. Annu Rev Pharmacol Toxicol 53: 401-426, 2013.
50. Lan T, Hu Y, Hu F, Li H, Chen Y, Zhang J, Yu Y, Jiang S, Weng Q, Tian S, *et al*: Hepatocyte glutathione S-transferase mu 2 prevents non-alcoholic steatohepatitis by suppressing ASK1 signaling. J Hepatol 76: 407-419, 2022.
51. Sadrkhanloo M, Entezari M, Orouei S, Zabolian A, Mirzaie A, Maghsoudloo A, Raesi R, Asadi N, Hashemi M, Zarrabi A, *et al*: Targeting Nrf2 in ischemia-reperfusion alleviation: From signaling networks to therapeutic targeting. Life Sci 300: 120561, 2022.
52. Chanas SA, Jiang Q, McMahon M, McWalter GK, McLellan LI, Elcombe CR, Henderson CJ, Wolf CR, Moffat GJ, Itoh K, *et al*: Loss of the Nrf2 transcription factor causes a marked reduction in constitutive and inducible expression of the glutathione S-transferase Gsta1, Gsta2, Gstm1, Gstm2, Gstm3 and Gstm4 genes in the livers of male and female mice. Biochem J 365(Pt 2): 405-416, 2002.
53. Saw CL, Yang AY, Guo Y and Kong AN: Astaxanthin and omega-3 fatty acids individually and in combination protect against oxidative stress via the Nrf2-ARE pathway. Food Chem Toxicol 62: 869-875, 2013.
54. Wang L, Zhao M, Qian R, Wang M, Bao Q, Chen X, Du W, Zhang L, Ye T, Xie Y, *et al*: Nicotinamide mononucleotide ameliorates silica-induced lung injury through the Nrf2-Regulated glutathione metabolism pathway in mice. Nutrients 15: 143, 2022.
55. Zou W, Chen C, Zhong Y, An J, Zhang X, Yu Y, Yu Z and Fu J: PI3K/Akt pathway mediates Nrf2/ARE activation in human L02 hepatocytes exposed to low-concentration HBCDs. Environ Sci Technol 47: 12434-12440, 2013.
56. Ali T, Kim T, Rehman SU, Khan MS, Amin FU, Khan M, Ikram M and Kim MO: Natural dietary supplementation of anthocyanins via PI3K/Akt/Nrf2/HO-1 pathways mitigate oxidative stress, neurodegeneration, and memory impairment in a mouse model of Alzheimer's disease. Mol Neurobiol 55: 6076-6093, 2018.